Science
AAAS

Supplementary Materials for

Constraints on the adjustment of tidal marshes to accelerating sea level rise

Neil Saintilan *et al*.

Corresponding author: Neil Saintilan, neil.saintilan@mq.edu.au

Science **377**, 523 (2022)
DOI: 10.1126/science.abo7872

The PDF file includes:

Other Supplementary Material for this manuscript includes the following:

Materials and Methods

1. Conceptual Model

We conceptualise surface elevation trends as a function of elevation gains (through mineral and organic matter accumulation, and soil volume expansion, including root mass gain) and losses (through sediment erosion, and soil volume losses associated with subsidence, autocompaction and decomposition of organic matter). These processes are driven by hydrological, geomorphological and biological contributions (Fig 1). Hydrological processes influence the accumulation of sediment through the mechanism of tidal inundation. Tides define the lateral limit of tidal marshes and the space available for accumulation of both mineral and organic matter, and accumulation of tidally-borne matter on marsh surfaces is also a function of inundation depth. Sea-level rise alters the elevation of tides and consequently influences both accommodation space and the rate of vertical accretion occurring on marsh surfaces. Geomorphological processes influence the suspended sediment supply, sediment characteristics and the rate of shallow subsidence. Biological processes include the influence of vegetation on sediment trapping and below-ground root production, and the influence of microbial decomposition on soil organic matter concentrations and volumes (*32*). Climate (temperature and precipitation) influences biological processes including plant productivity and microbiological activity. Identifiers and variables used in the analysis are provided in Table S2.

2. SET-MH network and installation

The Surface Elevation Table-Marker Horizon (SET-MH (*33*)) technique is the global standard for measuring wetland responses to sea-level rise in real time (*18*). It combines a benchmark rod and detachable arm against which marsh elevation change is repeatedly monitored (the SET), with an artificial marker horizon against which marsh vertical accretion is measured (the MH) (*34*) (Fig 1). Prior to installation, a platform is usually constructed around the monitoring site to minimise disturbance and compaction. In our network, two types of benchmark rod were used: the "original" design consisting of a hollow aluminium tube (~ 7.5 cm dia.) up to 8 m in length, and an "rSET" design, consisting of a stainless-steel rod (~ 1.5 cm dia.) capable of insertion to greater depths (up to ~30 m). In both cases the base of the benchmark rods serve as a fixed point against which marsh elevation change is measured. The portable SET arm is attached to the benchmark at each visitation and nine replicate pins are lowered to the marsh surface at four fixed bearings; measurements of the height of each pin above the portable arm are taken at each visit. At commencement, replicate (3 to 4) marker horizons (feldspar, clay or similar distinguishable material) were laid on the marsh surface within 0.25 m^2 square plots adjacent to each SET, and these MH were subsequently buried by the accumulation of tidally-borne sediments and in situ root growth. A shallow core is extracted and the depth of the marker horizon in each replicate plot recorded at each visit. The difference between surface accretion, as measured from cores extracted from the MH, and surface elevation change, as measured using the SET, is a measure of shallow subsidence or expansion occurring between the bottom of the marker horizon and base of the SET benchmark (*34*) (Fig 1). The SET pin measures have a reported accuracy of 1.3-4.3mm under field conditions (*35*).

Our network consists of 477 SET-MH monitoring stations in tidal marshes installed using common protocols in 97 locations and across four continents (North America, Australia, Europe, Africa). From this network, changes in surface elevation and vertical accretion were determined from repeated measurements at regular intervals across total record lengths ranging from 3.5 to

20 yr (average 10.1 yr: Data S1). This allowed quantification of rates of surface elevation change, and, where possible, vertical accretion at each site (see Section 8 below). The network may be characterised on the basis of geographic and geomorphic context (Table S1): Group I (Bay of Fundy Canada, UK east coast, Scheldt estuary Belgium) characterised by relatively stable late Holocene sea-level, and all of which are by coincidence macrotidal. Group II, consisting of regions experiencing consistent RSLR during the Holocene and includes the Atlantic and North Pacific US coast. Group III experienced slow RSLR through the late Holocene, and includes the Gulf of Mexico, southern California and the Mediterranean. These are subdivided in Table 1 between large deltas (the Mississippi, USA and Ebro, Spain: Group IIIa) and lagoonal settings (Group IIIb). Group IV includes far-field locations subject to stable or declining sea-level during the late Holocene and is represented by SE Australia and South Africa.

Tidal marsh SET-MH stations were not included in analyses when the length of the measurement record was short and potentially influenced by perturbations (minimum 3.5 yr), were not intertidal, where marsh elevation in relation to the tidal frame was not known, or where the SET-MH station was associated with a hydrological restoration initiative. Some sites had not recorded accretion but were included in analyses of elevation change. Sites spanned macrotidal settings (greater than 3 m tidal range: Bay of Fundy, Canada; Gulf of Maine, US; The Wash, UK) to microtidal settings (less than 1 m tidal range: US Gulf Coast; Venice Lagoon) and were distributed between coastlines subject to relatively rapid RSLR (>5 mm yr^{-1}; 122 SETs), near average global eustatic RSLR (2-5 mm yr^{-1}; 233 SETs), and low RSLR (<2 mm yr^{-1}; 122 SETs) averaged for the past 50 yr.

3. Position in tidal frame, elevation capital and time to failure

We measured the elevation (Z) of each SET-MH station in relation to the local height datum using either a real time kinematic GPS or differential GPS, and accessed mean high water (MHW), mean low water (MLW) and mean sea level (MSL) data in relation to the local height datum from the nearest tide gauge (Data S1; Table S3). We calculated tide range as the difference between MHW and MLW. We described position within the tidal frame using "dimensionless d" (*7*) (D; Equation 1), a metric increasingly used in the interpretation of intertidal position (*24*)·(*36*), and a a useful indicator of flooding duration (*36*).

$$D = \frac{(MHW - Z)}{(MHW - MLW)} \quad (1)$$

The elevation of a marsh in relation to the lowest elevation at which the plant species can survive has been termed "elevation capital" (*37*), and is useful for conceptualising the short-term vulnerability of vegetation to drowning under RSLR. (*20, 38*). Vegetation growth range can be normalised across sites of varying tidal range given the consistency of upper range limits in relation to MHW and lower range limits in relation to MSL for tidal marshes. We used the results of a global assessment of marsh lower limits (*39*) to relate lowest possible elevation to tidal range (Equation 2), whereby marsh tidal flat border relative to mean high water (Pio_h, cm) was described relative to mean tidal range (MTR).

$$P_{ioh} = -108.23 \times \log 10(MTR) + 163.21 \quad (2)$$

Elevation capital (elevCapital) was calculated as the difference between marsh elevation and the modelled marsh-tidal flat border (Pio_h). The time taken for marshes to submerge to a point that emergent vegetation cover could not be sustained we call "time to failure". This was calculated as the elevation capital divided by the elevation deficit, the difference between elevation and RSLR. We acknowledge the caveat that factors other than elevation may influence the survival of marsh vegetation in the context of high rates of RSLR, including for example the effect of topographic constraints on marsh drainage and hydroperiod (*40*), the influence of wave fields on lateral erosion (*41*), and species specific variation in inundation tolerance. The results are used for the purpose of broad-scale comparisons of vulnerability.

4. Relative sea-level rise

Contemporary rates of RSLR were obtained from the National Oceanic and Atmospheric Administration (NOAA) (https://tidesandcurrents.noaa.gov/sltrends/sltrends.html), or local tide gauges, as documented in Table S1. From the tide gauge data, we derived two measures of RSLR. First, we calculated the 50-year linear trend, to facilitate comparisons of RSLR between sites over a standard period. Second, we calculated the linear trend for the same period over which SET-MH stations were measured at each location. This we termed the "contemporaneous rate". The contemporaneous rate was in most settings higher than the 50-year rate (Data S1), as expected under accelerating RSLR(*42*), but is likely to be more influenced by regional climate drivers and the lunar nodal cycle(*43*) than the 50-year trend.

We also considered longer-term (centennial to millennial) rates of RSLR given the possible influence of past sea-level history on upper marsh processes. Rates of local and regional RSL change during the Holocene were primarily the result of glacio-isostatic adjustment (GIA), the ongoing deformational, rotational and gravitational effects on the Earth in response to the redistribution of ice and ocean loads that influences both eustatic and relative sea level. We use a revised numerical simulation of glacio-isostatic adjustment (*44*), which adopts the ICE-6G global ice reconstruction from the Last Glacial Maximum (LGM) to the present (*45, 46*). The GIA calculations are based on a gravitationally self-consistent theory for computing patterns of sea level. The model incorporates time-varying shorelines and the feedback of load-induced perturbations to Earth's rotation vector (*47*). The sea-level calculations were based on a gravitationally self-consistent theory that assumes a spherically symmetric, self-gravitating, Maxwell viscoelastic Earth model and adopts the ICE-6G global ice reconstruction (slightly modified from (*44*)). The elastic and density components of the model were given by the seismically inferred earth model PREM (*48*) and the Earth's structure was characterised by three parameters: the lithospheric thickness, *LT*, and upper and lower mantle viscosities denoted by V_{UM} and V_{LM}, respectively.

We used an ensemble of 300 combinations of these rheological parameters in the Glacio-Isostatic Adjustment (GIA) model to estimate RSL at 500-yr periods on a 512 x 260 global grid (Data S1). The 300 combinations of parameters included *LT* from 24 – 140 km, V_{UM} from 0.3 – 2 x 10^{21} Pas, and V_{LM} from 3 – 100 x 10^{21} Pas, where each combination was assumed to be equally likely. We linearly interpolated between grid and time points from these ensemble members to predict rates of RSL change and the uncertainties for each site in this study. Rates of historic change were calculated as a linear trend from 3000-0 BP (SLR3000 in Table S1; Data S1).

5. Background suspended sediment concentration (total suspended matter TSM)

A remote sensing product that estimates the dry weight of particles suspended in the coastal water column (g m^3) was compared to field measurements of vertical accretion, similar to previous studies (*4, 11, 20, 49*). Data collected by MEdium Resolution Imaging Spectrometer (MERIS) instrument (290-1040 nm) on the ENVISAT satellite, hosted by the European Space Agency (ESA)(*50*) were processed and validated through the ESA's GlobColour (downloadable from http://hermes.acri.fr/). TSM data were level-3 processed at 4 km^2 resolution in Plate Carrée projection. Data were binned monthly from January to December 2011 (the most recent year of data available), and the mean monthly values were used to generate an annual average TSM product. 85% of SET sites comprised 11-12 months of TSM data, 10% of sites comprised 9-10 months of TSM data, and 5% of sites comprised 8 months or less of TSM data. At the time of extraction, data were available from 2002-2011, though a previous study has shown that spatial variation in TSM shown in 2011 is representative of spatial variation across the entire time period (*20*).

The open-source software BEAM VISAT was used to extract TSM data from the pixel encompassing a SET site (78.4% of sites), or the closest pixel (21.6% of sites). For the latter, this was generally the neighbouring pixel, though the farthest TSM pixels (Scheldt Estuary, Belgium) were 6 pixels (24 km) away from the SET site. GlobColour TSM values are only indicative of variations in TSM locally in the considered marsh sites and may poorly estimate the local-scale resuspension and delivery of sediment in marsh environments, or pulse depositional events associated with high magnitude episodic events.

6. Climate, vegetation, soil properties and geomorphic setting

Mean annual temperature and mean annual precipitation were sourced from the nearest meteorological station, as documented in Table S3. Dry bulk density is the dry weight of both organic and inorganic materials in a sample of known volume, and typically reported as g cm^{-3} (*51*). We measured the dry bulk density of the upper 10 cm, the section of profile most likely to correspond to sediment accreted during the period of record. The percentage of organic matter within this soil depth was measured for most SET-MH monitoring sites (n= 325). Dominant vegetation was classified to genus level (Data S1), and clustered into the following categories by growth form and habit:

- *Spartina (Sporobolus)* (most frequently the dominant genus)
- Short grasses and herbs*: Sporobolus (Spartina), Distichlis, Salicornia, Sarcocornia, Poa, Glaux, Borrichia, Puccinellia, Paspalum, Elymus, Impatiens*
- Brackish rushes: *Juncus, Schoenoplectus, Phragmites, Cladium, Scirpus, Carex,*
- Saltbushes/shrubs: *Atriplex, Tecticornia,* and a stunted growth form of the mangrove *Avicennia*

Sites were classified according to the geomorphic units using a typology that defines estuarine settings on the basis of dominance of river, wave and tide energy (*52-54*): barrier estuarine (estuaries sheltered behind sand barriers along wave-dominated coastlines); riverine estuarine (sites associated with river systems where fluvial sedimentation is building active deltas); tidal estuarine (sites of meso-macro tidal range in which tidal deposition and erosion is a dominant process); calcareous (sites associated with coral reef barriers); and marine embayment (sites protected from oceanic waves by shoreline configuration but for which fluvial influence is

minor). Dominant vegetation categories and geomorphic units were used as categorical predictors in RandomForest classifications (see below).

7. Shoreline trend assessment and ratios of unvegetated to vegetated marsh (UVVR)

We used Google Earth Engine to locate the position of SET monitoring stations. The monitoring stations were used as a fixed point in the landscape against which to assess shoreline change. The distance between the SET monitoring station and the nearest vegetated shoreline was measured over the period for which available historic imagery corresponded most closely to the length of the SET record. For Australian sites, where mangroves frequently occupy the lower intertidal zone, the distance to the closest contiguous mangrove stand was also measured. Imagery was discarded if high water level or cloud cover obscured the platform or vegetated shoreline. In some cases, georectification errors prevented meaningful comparison between images. Results are shown in Table S1.

The ratio of unvegetated to vegetated marsh (UVVR) has been identified as a useful indicator of marsh stability (*28, 55*). Stable marshes are presumed to be more likely to be uniformly vegetated, and the UVVR can provide a snapshot of the status of a marsh on a spectrum towards conversion to open water. A UVVR of <0.15 is characteristic of intact marshes showing little deterioration (*56*). We calculated UVVR within a one-hectare perimeter of each SET-MH monitoring station using the most recent imagery archived on Google Earth Engine. We included open water in the assessment of UVVR.

8. Data Analysis

For each SET monitoring station, relative pin height was calculated by subtracting baseline pin height from all subsequent measurements. Relative pin heights were averaged hierarchically within each SET arm position and then across positions to integrate small-scale variation in surface elevation. The rate of elevation change was then calculated as a linear regression pin height against time. A similar approach was used to calculate accretion rates. Simple and multiple linear regression analyses were used to test relationships among quantitative variables. Generalized additive models (GAM) were used to test the relationship between subsidence and accretion rate. Analysis of variance was used to compare the rate of accretion and surface elevation gain between retreating and advancing marshes low and high in the tidal frame (D), and soil organic carbon concentrations across groups defined in Table S1.

RandomForest (RF) classifications (*57*) were used to examine relationships among accretion, surface elevation change, shoreline retreat, UVVR, and all other predictor variables (Table S1). RF is a machine learning approach which operates by constructing thousands (n = 10,000) of small classification trees, results of which are then tallied across the entire forest. An unbiased estimate of error is obtained at each step internally by using a different bootstrap resample from the original data. Approximately 33% of observations were used to test each classification's performance as the out-of-bag error (OOB). Data compilation, analyses and visualizations were undertaken in R (version 4.0.2 (*58*)) using *tidyr* (*59*), *randomForest (60)* and *viridis* (*59*) packages.

To estimate the probability of a deficit between elevation gain and RSLR, we follow ref (*12*) by converting the deficits to binary response variables (positive deficit = 1, negative = 0, and stable (within +/- 1 mm deficit) randomly assigned to 1 or 0). We summarize the probability of a deficit by modelling their relationship with contemporaneous rates of RSLR in a Bayesian

framework. We find that when rates of RSLR are > 6.0 mm yr^{-1}, the probability of a positive elevation deficit increases to ~90% (95% uncertainty interval (UI): 86.8% to 95.5%), making tidal marshes vulnerable to drowning.

Fig S1: **Marsh vulnerability in minerogenic and organic settings**. The relationships between accretion and RSLR (A), and with increasing depth in the tidal frame (B), and the rate of shallow marsh subsidence and vertical accretion (C), suppressing elevation adjustment to RSLR (D) as in Fig 3 but separated for minerogenic and organic marsh settings. In panels (B) and (C) points are coloured for the 50-year RSLR trend in mm yr^{-1}, and in (D) for estimated time to failure (yr) under the elevation deficit against the 50-yr RSLR trend (*19*).

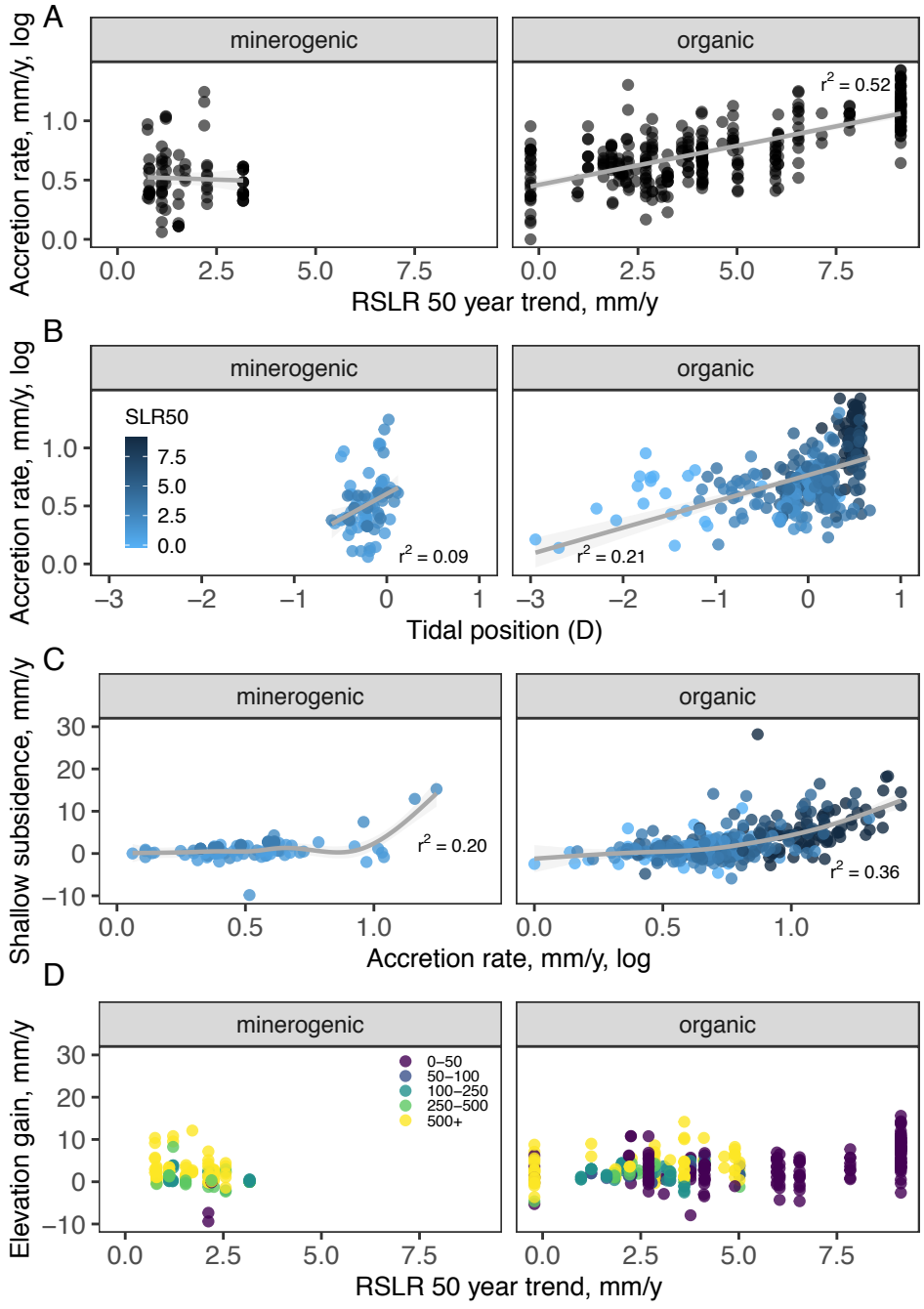

Fig S2: The relative importance of variables contributing to accretion model based on Random Forests analyses; total percentage of variation explained by the model is included in the plot title. Variable importance shows the mean increase in mean standard error (MSE) that variable contributes divided by its variability, it is thus possible to obtain MSE increase > 100% (e.g., as with Cohen's d) and this variable importance is not equivalent to R^2. Colour is used to highlight the predictors of increasing importance from light to dark. Top 15 predictors are shown. Variables used as explained in Table S1 (from Data S1).

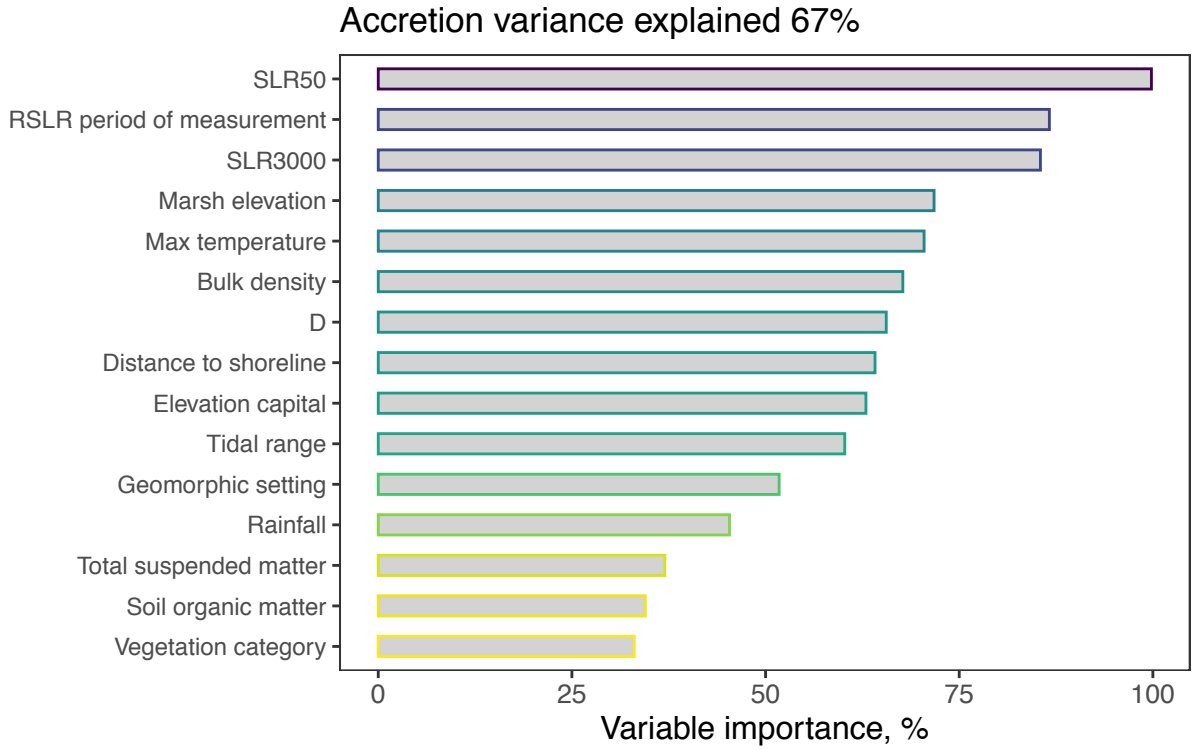

Fig S3.

The relative importance of variables contributing to models of marsh surface elevation and subsidence at global scales, based on Random Forests analyses. The total percentage of variation explained by the model is included in plot title. Variables used as explained in Table S1 (from Data S1).

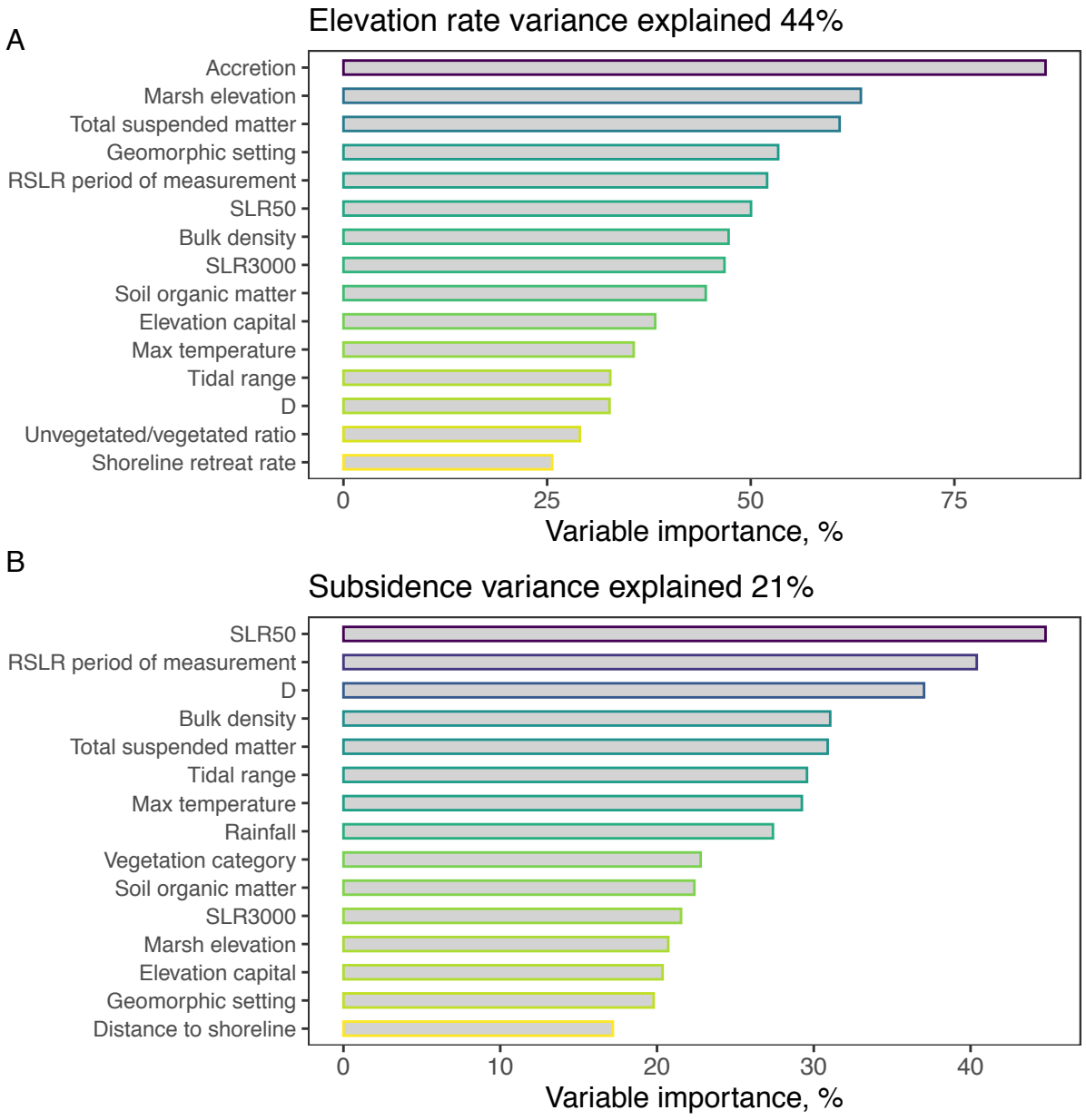

Fig S4.

High rates of elevation gain are associated with proximity to shorelines, particularly in microtidal settings.

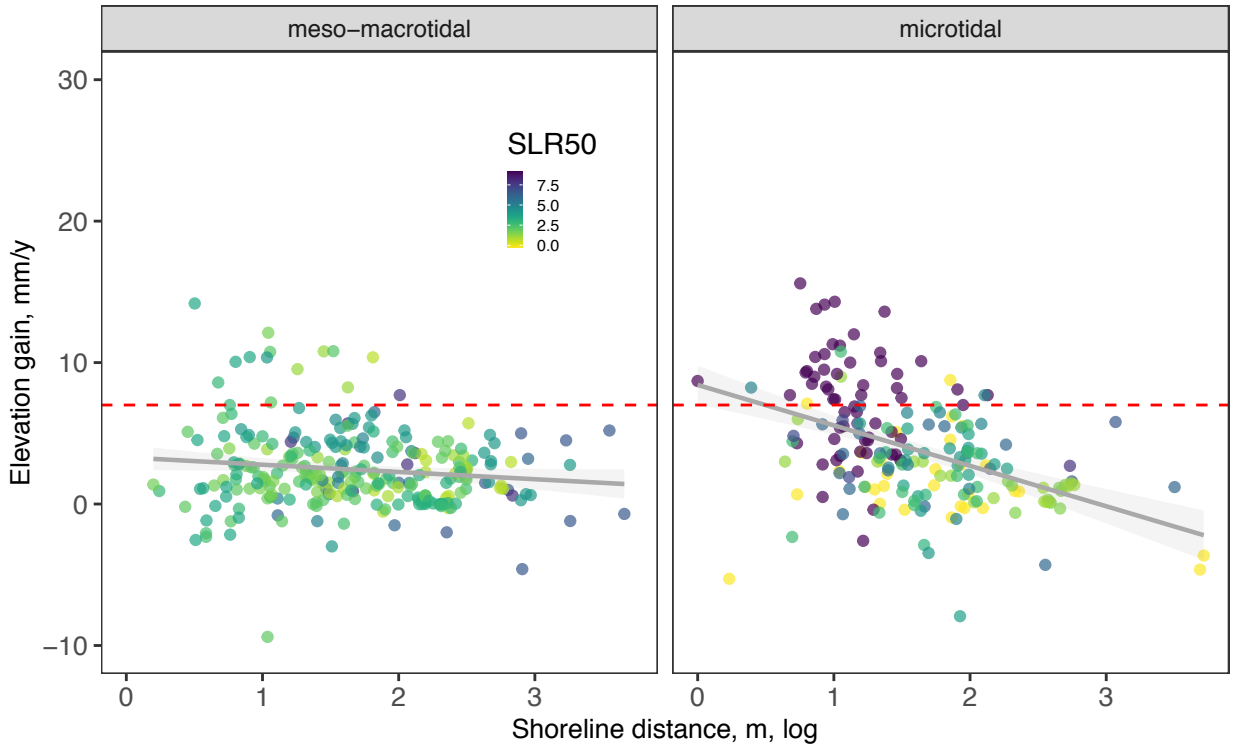

Fig S5

Two SET-MH stations subject to erosion during the measurement period, illustrating the short-term increase in elevation gain prior to failure. The parallel planks of the SET platforms are visible. Data retrieved from the Coastal Information Management System (CIMS) database (http://cims.coastal.louisiana.gov) with images from Google Earth: CRMS 347 (29.16397N; 90.69962W) and CRMS 302 (29.14783N; 90.91699W).

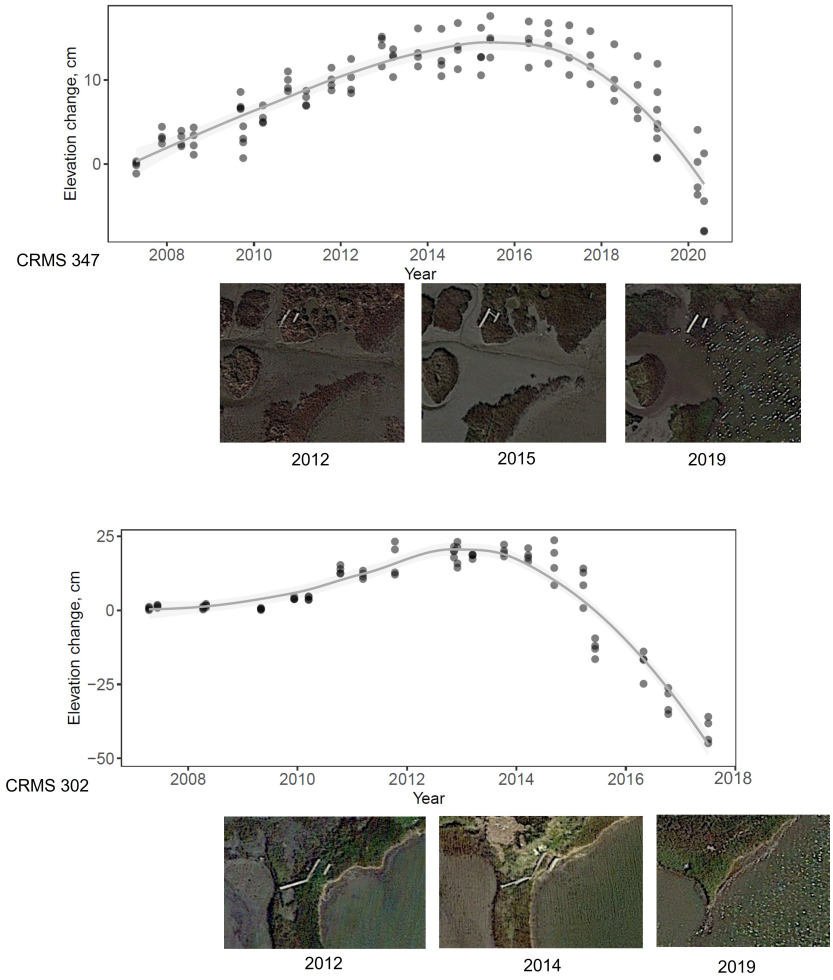

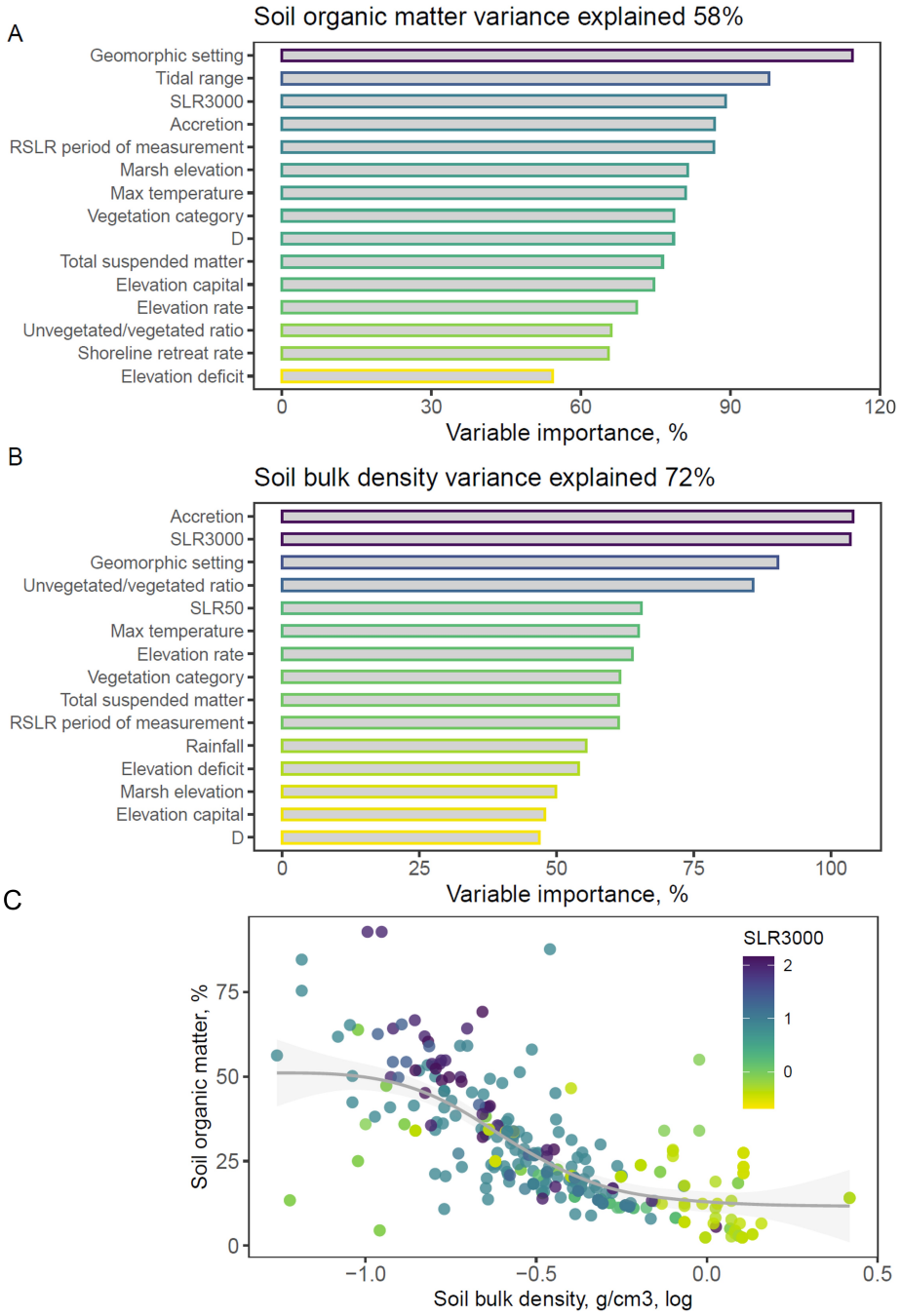

Fig. S6.

The relative importance of variables contributing to models of percent organic matter (a) and soil bulk density (b) at the global scale, based on Random Forests analyses. The total percentage of variation explained by the model is included in plot title. The proportional contribution of organic matter to accreting sediment is inversely related to bulk density (c). An decrease in bulk density is associated with sites subject to an historic (0-3000 year) rising sea-level trend.

Table S1.

Indicators of regional saltmarsh vulnerability to sea-level rise. Values are means of the number of sites (n) with standard deviation in parentheses. UVVR is the Unvegetated:Vegetated ratio. Local Relative Sea Level Rise (RSLR) is calculated for the previous 3000 years using Glacio-isostatic adjustment modelling; and for 50 years prior to 2021 (RSLR 0-50) and for the period contemporaneous with site SET-MH measurements (RSLR SET period) using tide gauges. Group I (Bay of Fundy Canada, UK east coast, Scheldt estuary Belgium). Group II, late Holocene RSLR including Atlantic and North Pacific US coast. Group III: slow late Holocene RSLR including the Gulf of Mexico, southern California and the Mediterranean (large deltas Group IIIA, lagoonal Group IIIB). Group IV SE Australia and South Africa.

a: Pressure variables

Group (n)	Elevation above lower limit (cm)	Tide range (m)	RSLR 0-3000 (mm yr^{-1})	RSLR 0-50 (mm yr^{-1})	RSLR Contemp. (mm yr^{-1})	Total Suspended Matter (mg l^{-1})
I (50)	180.9 (61.7)	4.31 (2.55)	0.44 (0.56)	1.93 (0.6)	3.05 (4.49)	12.5 (10.4)
II (117)	26.9 (43.2)	1.5 (1.20)	0.88 (1.03)	3.88 (1.15)	4.76 (3.15)	6.3 (6.7)
IIIa (94)	7.9 (20.5)	0.54 (0.24)	0.56 (0.44)	6.15 (4.38)	8.8 (7.9)	7.9 (4.6)
IIIb (144)	24.6 (34.9)	1.04 (0.37)	0.92 (0.60)	3.67 (2.00)	10.44 (7.03)	10.0 (8.0)
IV (72)	92.7 (35.5)	1.41 (0.43)	-0.39 (0.06)	1.84 (0.89)	3.00 (0.95)	4.3 (3.8)

b. Response variables

Group	Sediment Organic Matter %	Dry Bulk Density g/cm_3	Sediment Accretion (mm yr^{-1})	Subsidence (mm yr^{-1})	Elevation gain (mm yr^{-1})	Elevation Deficit (mm yr^{-1})	Shoreline trend (m yr^{-1})	UVVR
I	14.1 (6.5)	0.53 (0.18)	4.9 (4.1)	1.2 (4.6)	2.8 (3.2)	0.3 (4.7)	0.56 (1.96)	0.14 (0.08)
II	42.7 (19.5)	0.28 (0.19)	3.9 (2.1)	1.1 (2.7)	2.9 (2.6)	1.8 (4.5)	-0.31 (0.39)	0.22 (0.2)
IIIa	25.2 (12.6)	0.37 (0.27)	9.8 (6.3)	5.1 (9.0)	4.9 (5.8)	3.8 (7.7)	-0.13 (0.32)	0.32 (0.22)
IIIb	32.5 (17.6)	0.40 (0.23)	5.0 (3.5)	2.3 (3.8)	2.7 (3.2)	7.7 (7.6)	-0.34 (0.62)	0.23 (0.23)

IV	15.2 (11.2)	0.89 (0.39)	1.9 (1.0)	1.0 (1.1)	0.8 (2.1)	2.2 (2.5)	-0.01 (0.42)	0.10 (0.15)

Table S2.
Identifiers and Variables used in the analysis (Data S1).

site.SET.identifier	Unique SET station ID used for linking all other data
Network	Geographic clusters of SETs
Country	Country within which SET is situated
site.label	Site name for SET or replicate SETs
Latitude	Decimal degrees
longitude	Decimal degrees
SLR.Zone	Location in relation to millennial-scale RSLR history
startDate	Initial SET reading
endDate	Final SET reading
Years	Time record for the SET readings (yr)
accretion	Rate of accretion above the feldspar horizon (mm yr^{-1})
elevation.rate	Rate of elevation gain from the SET record (mm yr^{-1})
Subsidence	accretion -elevation.rate
R2.SET	R^2 of the linear trend in elevation through time
SLR50	Local sea-level trend derived from nearest tide gauge: 0-50BP linear trend (mm yr^{-1})
RSLR.contemporaneous	RSLR for each site for the period of SET measurement. Linear trend (mm yr^{-1})
SLR3000	Sea level trend 0 - 3000 BP (from Glacio-isostatic modelling) (mm yr^{-1})
MHW	Mean High Water: datum consistent with marsh elevation (m)
MLW	Mean Low Water: datum consistent with marsh elevation (m)
MSL	Mean Sea Level: datum consistent with marsh elevation (m)
tidal.range	Difference between MHW and MLW (m)
marshElevation	Elevation of the SET in relation to local datum (m)
D	Dimensionless D, see (*19*) for equation
posTidalFrame	Elevation in relation to the difference between MHW and MLW (m)
elevCapital	Elevation of SET in relation to modelled lowest marsh limits (cm)

elevDeficit	Elevation Deficit, defined as RSLR period of measure minus elevation rate. (mm yr^{-1})
lowMarshLim	Modelled low marsh limit below MHW
lowMarshLimHeightDatum	Modelled low marsh limit below local height datum
bulkDensity	Bulk density of the upper 10 cm (dry, g cm^{-3})
Organic matter	Organic matter in the upper 10cm by weight (%)
maxTemp	Average daily maximum temperature (°C)
Rainfall	Average annual rainfall (mm)
TSM.2011	MERIS-derived total suspended matter -average
TSM.2011 STDEV	MERIS-derived total suspended matter -standard deviation
Dominant.vegetation	Dominant genus at the SET-MH installation
Spartina	Spartina dominant, binary
shortGrassesHerbs	dominated by short grasses and herbs (*Sporobolus/Spartina, Distichlis, Salicornia, Sarcocornia, Poa, Glaux, Borrichia, Puccinellia, Paspalum, Elymus, Impatiens*), binary
brackishRushes	dominated by brackish rushes (*Juncus, Schoenoplectus, Phragmites, Cladium, Scirpus, Carex*)
saltbushes	dominated by saltbushes or shrubs (*Atriplex, Tecticornia, Avicennia*)
category	Vegetation structural category
Geomorphic.setting	River deltaic, Tide Dominant, barrierLagoon, Barrier estuary, Embayment, Drowned River Valley
Shore.rate	rate of shoreline retreat m yr^{-1}
Shore.R2	R^2 of shoreline rate of change
Shore.Dist	distance to shoreline (m)
UVVR	unvegetated-to-vegetated ratio
TimeToFailure50	Projected time to marsh failure at current 50-year RLSR trend
Retreat.Failure	Projected time to SET erosion at current rates of lateral retreat

Table S3.

Sources of meteorological and sea-level data included in Data S1

Region	Climate Data	Tidal Data	RSL
United States	https://www.ncdc.noaa.gov/cdo-web/datatools/normals	https://tidesandcurrents.noaa.gov/map/index.html?type=TidePredictions&region=	https://tidesandcurrents.noaa.gov/sltrends/sltrends.html http://www.star.nesdis.noaa.gov/sod/lsa/SeaLevelRise/
United Kingdom	https://www.metoffice.gov.uk/research/climate/maps-and-data/uk-climate-averages	https://www.ntslf.org/data/uk-network-real-time	https://tidesandcurrents.noaa.gov/sltrends/sltrends.html http://www.star.nesdis.noaa.gov/sod/lsa/SeaLevelRise/
Canada	https://climate.weather.gc.ca/climate_normals/	https://protect-au.mimecast.com/s/4wJnCE8wlRCKAKNMSNvEdI?domain=meds-sdmm.dfo-mpo.gc.ca	https://tidesandcurrents.noaa.gov/sltrends/sltrends.html http://www.star.nesdis.noaa.gov/sod/lsa/SeaLevelRise/
Spain	https://en.climate-data.org/europe/spain/catalonia/deltebre-768271/		https://tidesandcurrents.noaa.gov/sltrends/sltrends.html Reference(*61*) http://www.star.nesdis.noaa.gov/sod/lsa/SeaLevelRise/
Australia	http://www.bom.gov.au/climate/data/index	New South Wales: https://s3-ap-southeast-2.amazonaws.com/www-data.manly.hydraulics.works/www/publications/TideCharts/2020TideCharts.pdf; Reference(*62*) Victoria: https://vrca.vic.gov.au/wp-content/uploads/2020/02/Tides-Tables-2020-web.pdf	https://tidesandcurrents.noaa.gov/sltrends/sltrends.html http://www.bom.gov.au/oceanography/projects/abslmp/data/monthly.shtml (Port Kembla, Stony Point) http://www.star.nesdis.noaa.gov/sod/lsa/SeaLevelRise/
South Africa		References(*63*) (*64*)	https://tidesandcurrents.noaa.gov/sltrends/sltrends.html http://www.star.nesdis.noaa.gov/sod/lsa/SeaLevelRise/

Table S4.

Rates of elevation gain (mm yr^{-1}) and accretion (mm yr^{-1}) in relation to position in tidal frame and shoreline trends; standard deviation in parentheses. Statistical comparisons, separate for accretion and elevation, are based on the ANOVA with four levels of factor combinations (two levels of "dimensionless D" (*7*) and two levels of shoreline trend, retreating vs. advancing) with Tukey post-hoc comparisons.

	Global average	Low Marsh (D>0)			High Marsh (D<0)		
		Advance	Stable	Retreat	Advance	Stable	Retreat
Elevation	2.92 (3.80)	2.94 (2.98)^{ab}	3.96 (4.83)^{b}	5.04 (4.11)^{b}	1.95 (2.84)^{a}	2.47 (3.11)^{ab}	1.15 (1.92)^{a}
Accretion	5.33 (4.58)	6.42 (3.69)^{b}	7.76 (5.49)^{b}	8.75 (6.47)^{b}	2.82 (2.35)^{a}	3.15 (1.93)^{a}	3.37 (2.76)^{a}

Table S5.

Median projected time to failure at SET-MH stations, calculated as the time taken to reach minimum survival elevation under the current (contemporaneous) elevation deficit (elevation failure), and the time taken to erode the wetland surface at the SET-MH station under current rates of retreat (retreat failure). Retreat rate is extrapolated from current rates and does not model changes to open water fetch, likely to be an important determinant would be influenced by open water fetch(*65*). Note that the median projected survival time is lower under *higher* rates of elevation gain. SET-MH stations with >7mm yr^{-1} elevation gain are immediately adjacent to retreating shorelines, suggesting the formation of an incipient, temporary levee bank.

Surface Elevation rate of change (mm yr^{-1})	n	Distance to shore (m)	Elevation failure (median years)	Retreat failure (median years)
>7	58	22.7 (29.6)	2.5	74.1
3.5-7	122	121.8 (376.8)	62	127.4
1.5-3.5	119	124.3 (221.2)	127.9	623.7
0-1.5	115	192.2 (348.1)	130.8	>1000
<0	63	354.7 (1070.2)	99.3	>1000

References and Notes

1. N. C. Davidson, How much wetland has the world lost? Long-term and recent trends in global wetland area. *Mar. Freshw. Res.* **65**, 934–941 (2014).

2. N. J. Murray, T. A. Worthington, P. Bunting, S. Duce, V. Hagger, C. E. Lovelock, R. Lucas, M. I. Saunders, M. Sheaves, M. Spalding, N. J. Waltham, M. B. Lyons, High-resolution mapping of losses and gains of Earth's tidal wetlands. *Science* **376**, 744–749 (2022).

3. R. Costanza, R. de Groot, P. Sutton, S. van der Ploeg, S. J. Anderson, I. Kubiszewski, S. Farber, R. K. Turner, Changes in the global value of ecosystem services. *Glob. Environ. Change* **26**, 152–158 (2014).

4. S. Fagherazzi, G. Mariotti, N. Leonardi, A. Canestrelli, W. Nardin, W. S. Kearney, Salt Marsh Dynamics in a Period of Accelerated Sea Level Rise. *J. Geophys. Res.* **125**, e2019JF005200 (2020).

5. M. Schuerch, T. Spencer, S. Temmerman, M. L. Kirwan, C. Wolff, D. Lincke, C. J. McOwen, M. D. Pickering, R. Reef, A. T. Vafeidis, J. Hinkel, R. J. Nicholls, S. Brown, Future response of global coastal wetlands to sea-level rise. *Nature* **561**, 231–234 (2018).

6. M. L. Kirwan, J. P. Megonigal, Tidal wetland stability in the face of human impacts and sea-level rise. *Nature* **504**, 53–60 (2013).

7. M. L. Kirwan, S. Temmerman, E. E. Skeehan, G. R. Guntenspergen, S. Fagherazzi, Overestimation of marsh vulnerability to sea level rise. *Nat. Clim. Change* **6**, 253–260 (2016).

8. J. T. Morris, P. Sundareshwar, C. T. Nietch, B. Kjerfve, D. R. Cahoon, Responses of coastal wetlands to rising sea level. *Ecology* **83**, 2869–2877 (2002).

9. J. French, Tidal marsh sedimentation and resilience to environmental change: Exploratory modelling of tidal, sea-level and sediment supply forcing in predominantly allochthonous systems. *Mar. Geol.* **235**, 119–136 (2006).

10. N. Saintilan, N. S. Khan, E. Ashe, J. J. Kelleway, K. Rogers, C. D. Woodroffe, B. P. Horton, Thresholds of mangrove survival under rapid sea level rise. *Science* **368**, 1118–1121 (2020).

11. M. L. Kirwan, G. R. Guntenspergen, A. D'Alpaos, J. T. Morris, S. M. Mudd, S. Temmerman, Limits on the adaptability of coastal marshes to rising sea level. *Geophys. Res. Lett.* **37**, L23401 (2010).

12. D. J. Coleman, M. Schuerch, S. Temmerman, G. Guntenspergen, C. G. Smith, M. L. Kirwan, Reconciling models and measurements of marsh vulnerability to sea level rise. *Limnol. Oceanogr. Lett.* **7**, 140–149 (2022).

13. B. P. Horton, I. Shennan, S. L. Bradley, N. Cahill, M. Kirwan, R. E. Kopp, T. A. Shaw, Predicting marsh vulnerability to sea-level rise using Holocene relative sea-level data. *Nat. Commun.* **9**, 2687 (2018).

14. T. E. Törnqvist, K. L. Jankowski, Y.-X. Li, J. L. González, Tipping points of Mississippi Delta marshes due to accelerated sea-level rise. *Sci. Adv.* **6**, eaaz5512 (2020).

15. M. L. Kirwan, G. R. Guntenspergen, Influence of tidal range on the stability of coastal marshland. *J. Geophys. Res.* **115**, F02009 (2010).

16. J. P. Syvitski, A. Kettner, Sediment flux and the Anthropocene. *Philos. Trans. R. Soc. A* **369**, 957–975 (2011).

17. L. A. Deegan, D. S. Johnson, R. S. Warren, B. J. Peterson, J. W. Fleeger, S. Fagherazzi, W. M. Wollheim, Coastal eutrophication as a driver of salt marsh loss. *Nature* **490**, 388–392 (2012).

18. K. Rogers, J. J. Kelleway, N. Saintilan, J. P. Megonigal, J. B. Adams, J. R. Holmquist, M. Lu, L. Schile-Beers, A. Zawadzki, D. Mazumder, C. D. Woodroffe, Wetland carbon storage controlled by millennial-scale variation in relative sea-level rise. *Nature* **567**, 91–95 (2019).

19. E. L. Webb, D. A. Friess, K. W. Krauss, D. R. Cahoon, G. R. Guntenspergen, J. Phelps, A global standard for monitoring coastal wetland vulnerability to accelerated sea-level rise. *Nat. Clim. Change* **3**, 458–465 (2013).

20. See supplementary materials.

21. C. E. Lovelock, D. R. Cahoon, D. A. Friess, G. R. Guntenspergen, K. W. Krauss, R. Reef, K. Rogers, M. L. Saunders, F. Sidik, A. Swales, N. Saintilan, X. Thuyen, T. Triet, The

vulnerability of Indo-Pacific mangrove forests to sea-level rise. *Nature* **526**, 559–563 (2015).

22. K. L. Jankowski, T. E. Törnqvist, A. M. Fernandes, Vulnerability of Louisiana's coastal wetlands to present-day rates of relative sea-level rise. *Nat. Commun.* **8**, 14792 (2017).

23. C. E. Lovelock, R. Reef, Variable Impacts of Climate Change on Blue Carbon. *One Earth* **3**, 195–211 (2020).

24. F. Wang, C. J. Sanders, I. R. Santos, J. Tang, M. Schuerch, M. L. Kirwan, R. E. Kopp, K. Zhu, X. Li, J. Yuan, W. Liu, Z. Li, Global blue carbon accumulation in tidal wetlands increases with climate change. *Natl. Sci. Rev.* **8**, nwaa296 (2020).

25. B. Fox-Kemper, H. T. Hewitt, C. Xiao, G. Aðalgeirsdóttir, S. S. Drijfhout, T. L. Edwards, N. R. Golledge, M. Hemer, R. E. Kopp, G. Krinner, A. Mix, D. Notz, S. Nowicki, I. S. Nurhati, L. Ruiz, J.-B. Sallée, A. B. A. Slangen, Y. Yu, in *Climate Change 2021: The Physical Science Basis. Contribution of Working Group I to the Sixth Assessment Report of the Intergovernmental Panel on Climate Change*, V. Masson-Delmotte *et al*., Eds. (Cambridge Univ. Press, 2021), chap. 9.

26. J. T. Morris, Competition among marsh macrophytes by means of geomorphological displacement in the intertidal zone. *Estuar. Coast. Shelf Sci.* **69**, 395–402 (2006).

27. S. Nolte, E. C. Koppenaal, P. Esselink, K. S. Dijkema, M. Schuerch, A. V. De Groot, J. P. Bakker, S. Temmerman, Measuring sedimentation in tidal marshes: A review on methods and their applicability in biogeomorphological studies. *J. Coast. Conserv.* **17**, 301–325 (2013).

28. D. R. Cahoon, J. Day, D. Reed, The influence of surface and shallow subsurface soil processes on wetland elevation: A synthesis. *Curr. Top. Wetland Biogeochem.* **3**, 72–88 (1999).

29. N. K. Ganju, Z. Defne, M. L. Kirwan, S. Fagherazzi, A. D'Alpaos, L. Carniello, Spatially integrative metrics reveal hidden vulnerability of microtidal salt marshes. *Nat. Commun.* **8**, 14156 (2017).

30. J. L. Breithaupt, J. M. Smoak, T. S. Bianchi, D. R. Vaughn, C. J. Sanders, K. R. Radabaugh, M. J. Osland, L. C. Feher, J. C. Lynch, D. R. Cahoon, G. H. Anderson, K. R. T. Whelan,

B. E. Rosenheim, R. P. Moyer, L. G. Chambers, Increasing rates of carbon burial in southwest Florida coastal wetlands. *J. Geophys. Res.* **125**, e2019JG005349 (2020).

31. K. W. Krauss, K. L. McKee, C. E. Lovelock, D. R. Cahoon, N. Saintilan, R. Reef, L. Chen, How mangrove forests adjust to rising sea level. *New Phytol.* **202**, 19–34 (2014).

32. J. C. Lynch, P. Hensel, D. R. Cahoon, *The Surface Elevation Table and Marker Horizon Technique: A Protocol for Monitoring Wetland Elevation Dynamics* (National Park Service, 2015).

33. D. R. Cahoon, D. J. Reed, J. W. Day Jr., Estimating shallow subsidence in microtidal salt marshes of the southeastern United States: Kaye and Barghoorn revisited. *Mar. Geol.* **128**, 1–9 (1995).

34. D. R. Cahoon, J. C. Lynch, B. C. Perez, B. Segura, R. D. Holland, C. Stelly, G. Stephenson, P. Hensel, High-precision measurements of wetland sediment elevation: II. The rod surface elevation table. *J. Sediment. Res.* **72**, 734–739 (2002).

35. H. Kefelegn, Mathematical Formulations for Three Components of Hydroperiod in Tidal Wetlands. *Wetlands* **39**, 349–360 (2019).

36. D. R. Cahoon, G. R. Guntenspergen, Climate change, sea-level rise, and coastal wetlands. *Natl. Wetlands Newsl.* **32**, 8–12 (2010).

37. J. T. Morris, J. Lynch, K. A. Renken, S. Stevens, M. Tyrrell, H. Plaisted, Tidal and Hurricane Impacts on Saltmarshes in the Northeastern Coastal and Barrier Network: Theory and Empirical Results. *Estuaries Coasts* **43**, 1658–1671 (2020).

38. T. Balke, M. Stock, K. Jensen, T. J. Bouma, M. Kleyer, A global analysis of the seaward salt marsh extent: The importance of tidal range. *Water Resour. Res.* **52**, 3775–3786 (2016).

39. J. F. Rodríguez, P. M. Saco, S. Sandi, N. Saintilan, G. Riccardi, Potential increase in coastal wetland vulnerability to sea-level rise suggested by considering hydrodynamic attenuation effects. *Nat. Commun.* **8**, 16094 (2017).

40. G. Mariotti, J. Carr, Dual role of salt marsh retreat: Long-term loss and short-term resilience. *Water Resour. Res.* **50**, 2963–2974 (2014).

41. S. Dangendorf, C. Hay, F. M. Calafat, M. Marcos, C. G. Piecuch, K. Berk, J. Jensen, Persistent acceleration in global sea-level rise since the 1960s. *Nat. Clim. Chang.* **9**, 705–710 (2019).

42. D. Peng, E. M. Hill, A. J. Meltzner, A. D. Switzer, Tide gauge records show that the 18.61-year nodal tidal cycle can change high water levels by up to 30 cm. *J. Geophys. Res. Oceans* **124**, 736–749 (2019).

43. S. Dendy, J. Austermann, J. Creveling, J. Mitrovica, Sensitivity of Last Interglacial sea-level high stands to ice sheet configuration during Marine Isotope Stage 6. *Quat. Sci. Rev.* **171**, 234–244 (2017).

44. D. F. Argus, W. Peltier, R. Drummond, A. W. Moore, The Antarctica component of postglacial rebound model ICE-6G_C (VM5a) based on GPS positioning, exposure age dating of ice thicknesses, and relative sea level histories. *Geophys. J. Int.* **198**, 537–563 (2014).

45. W. R. Peltier, D. Argus, R. Drummond, Space geodesy constrains ice age terminal deglaciation: The global ICE-6G_C (VM5a) model. *J. Geophys. Res. Solid Earth* **120**, 450–487 (2015).

46. R. A. Kendall, J. X. Mitrovica, G. A. Milne, On post-glacial sea level–II. Numerical formulation and comparative results on spherically symmetric models. *Geophys. J. Int.* **161**, 679–706 (2005).

47. A. M. Dziewonski, D. L. Anderson, Preliminary reference Earth model. *Phys. Earth Planet. Inter.* **25**, 297–356 (1981).

48. Z. Liu, S. Fagherazzi, B. Cui, Success of coastal wetlands restoration is driven by sediment availability. *Commun. Earth Environ.* **2**, 44 (2021).

49. R. Doerffer, K. Sorensen, J. Aiken, MERIS potential for coastal zone applications. *Int. J. Remote Sens.* **20**, 1809–1818 (1999).

50. H. Wang *et al*., Determining the spatial variability of wetland soil bulk density, organic matter, and the conversion factor between organic matter and organic carbon across coastal Louisiana, USA. *J. Coast. Res.* **33**, 507–517 (2017).

51. R. W. Dalrymple, B. A. Zaitlin, R. Boyd, Estuarine facies models; conceptual basis and stratigraphic implications. *J. Sediment. Res.* **62**, 1130–1146 (1992).

52. T. A. Worthington, P. S. E. Zu Ermgassen, D. A. Friess, K. W. Krauss, C. E. Lovelock, J. Thorley, R. Tingey, C. D. Woodroffe, P. Bunting, N. Cormier, D. Lagomasino, R. Lucas, N. J. Murray, W. J. Sutherland, M. Spalding, A global biophysical typology of mangroves and its relevance for ecosystem structure and deforestation. *Sci. Rep.* **10**, 14652 (2020).

53. C. Woodroffe, in *Tropical Mangrove Ecosystems*, A. I. Robertson, D. M. Alongi, Eds. (AGU, 1993), chap. 2.

54. N. K. Ganju, Z. Defne, S. Fagherazzi, Are elevation and open-water conversion of salt marshes connected? *Geophys. Res. Lett.* **47**, e2019GL086703 (2020).

55. K. Wasson, N. K. Ganju, Z. Defne, C. Endris, T. Elsey-Quirk, K. M. Thorne, C. M. Freeman, G. Guntenspergen, D. J. Nowacki, K. B. Raposa, Understanding tidal marsh trajectories: Evaluation of multiple indicators of marsh persistence. *Environ. Res. Lett.* **14**, 124073 (2019).

56. L. Breiman, Random forests. *Mach. Learn.* **45**, 5–32 (2001).

57. *R* (R Foundation for Statistical Computing, 2020).

58. S. Garnier, N. Ross, B. Rudis, M. Sciaini, C. Scherer, viridis: Default color maps from 'matplotlib'. R package version 0.5. 1. *CRAN: The Comprehensive R Archive Network* (2018).

59. A. Liaw, M. Wiener, Classification and regression by randomForest. *R News* **2**, 18–22 (2002).

60. E. S. Yando, M. J. Osland, J. M. Willis, R. H. Day, K. W. Krauss, M. W. Hester, Salt marsh-mangrove ecotones: Using structural gradients to investigate the effects of woody plant encroachment on plant–soil interactions and ecosystem carbon pools. *J. Ecol.* **104**, 1020–1031 (2016).

61. C. Marrasé, J. Camí, F. Peters, Report on Climate Change and Health in Catalonia: Informe de la Secció de Ciències Biològiques de l'Institut d'Estudis Catalans. (2020).

62. E. Couriel, K. Alley, B. Modra, *OEH NSW Tidal Planes Analysis: 1990–2010 Harmonic Analysis* (Report MHL2053, Government of New South Wales, 2012).

63. J. Raw, J. Adams, T. Bornman, T. Riddin, M. Vanderklift, Vulnerability to sea-level rise and the potential for restoration to enhance blue carbon storage in salt marshes of an urban estuary. *Estuar. Coast. Shelf Sci.* **260**, 107495 (2021).

64. B. Maree, Structure and status of the intertidal wetlands of the Knysna Estuary. *Trans. R. Soc. S. Afr.* **55**, 163–176 (2000).

65. G. Mariotti, S. Fagherazzi, Critical width of tidal flats triggers marsh collapse in the absence of sea-level rise. *Proc. Natl. Acad. Sci. U.S.A.* **110**, 5353–5356 (2013).